

QED in $\bar{B} \rightarrow \bar{K} \ell^+ \ell^-$ LFU ratios: Theory versus Experiment, a Monte Carlo Study

Gino Isidori,¹ Davide Lancerini,¹ Saad Nabeebaccus,^{1,2} Roman Zwicky,³

¹*Department of Physics, Universität Zürich, Winterthurerstr. 190, CH-8057 Zürich, Switzerland*

²*Université Paris-Saclay, CNRS, IJCLab, 91405 Orsay, France*

³*Higgs Centre for Theoretical Physics, School of Physics and Astronomy, University of Edinburgh, Peter Guthrie Tait Road, King's Buildings, Edinburgh EH9 3FD, Scotland, UK*

E-mail: isidori@physik.uzh.ch, davide.lancierini@uzh.ch,
saad.nabeebaccus@ijclab.in2p3.fr, roman.zwicky@ed.ac.uk

ABSTRACT: Using analytic results obtained in a meson effective theory, that includes all infrared sensitive logs, we build a dedicated Monte Carlo framework to describe QED corrections in $\bar{B} \rightarrow \bar{K} \ell^+ \ell^-$ for a generic form factor. For the neutral mode $\bar{B}^0 \rightarrow \bar{K}^0 \ell^+ \ell^-$, we perform a detailed numerical comparison versus those obtained with the general-purpose photon-shower tool PHOTOS. The comparison indicates a good agreement, at the few per-mil level, when focusing on the rare mode only. In addition, our framework allows us to investigate the impact of the charmonium resonances. Interference effects, not described by PHOTOS in the experimental analysis, are found to be small in the dilepton invariant mass region $q^2 < 6 \text{ GeV}^2$, which is used to determine $R_{K^{(*)}}$. Using a semi-analytic framework we assess the full, rare and resonant, mode. Based thereupon, we discuss strategies to check the subtraction of the resonant mode, which has a sizeable impact at $q^2 \approx 6 \text{ GeV}^2$ in the electron mode.

Contents

1. Introduction	1
2. Monte Carlo Framework	3
2.1. Generalities	3
2.2. Basic strategy of the Monte Carlo approach	4
2.3. Numerical procedure	5
3. Direct Comparison with PHOTOS at the Short Distance Level	6
3.1. Parameterisation of the short distance amplitude	6
3.2. Comparison of our Monte Carlo with PHOTOS	7
4. Adding Long Distance (Charmonium Resonances)	10
4.1. Parameterisation of the charm amplitude	11
4.2. Study of the J/Ψ -resonance interference term in our Monte Carlo	12
4.3. J/Ψ and $\Psi(2S)$, including the resonant mode via a semi-analytic approach	14
5. Outlook and Conclusions	17
A. Kinematics	19
B. More Detail on the Charm Parameterisation	19
C. Supplementary plots	21
D. Values of f^{th} used in the Monte Carlo Simulations	21

1. Introduction

Within the Standard Model (SM), the Yukawa coupling is the only interaction that distinguishes the different fermion families. In the lepton sector, all the Yukawa couplings are small compared to the SM gauge couplings, giving rise to an approximate accidental symmetry known as Lepton Flavour Universality (LFU). This symmetry holds to a very good accuracy within the SM, especially for the two lightest families (e and μ), and it can be tested to high accuracy in B meson decays, where the kinematic effects due to light lepton masses are small (see e.g. Ref. [1, 2] for a review).

Particularly interesting in this respect are the μ/e LFU ratios in flavour changing neutral currents (FCNC) transitions [3], such as

$$R_K \Big|_{q_0^2 \in [q_1^2, q_2^2] \text{ GeV}^2} = \frac{\Gamma[\bar{B} \rightarrow \bar{K} \mu^+ \mu^-]}{\Gamma[\bar{B} \rightarrow \bar{K} e^+ e^-]} \Big|_{q_0^2 \in [q_1^2, q_2^2] \text{ GeV}^2} , \quad (1.1)$$

where $q_0^2 \equiv (p_B - p_K)^2$. In the SM, $R_K^{\text{SM}} \approx 1$ up to QED corrections [4, 5]. The current experimental determination is [6–8]

$$R_K|_{q_0^2 \in [1.1, 6] \text{ GeV}^2} = 0.846_{-0.039-0.012}^{+0.042+0.016}, \quad (1.2)$$

and exhibits a statistically significant deviation from the theory prediction. Similar tensions between data and SM predictions, albeit with smaller statistical significance, have been reported in the analogous quantities R_{K^*0} [9], $R_{K^{*+}}$ and R_{K_S} [10].

In this paper, we assess the robustness of the theoretical determination of R_K with respect to QED corrections, which provide the dominant source of LFU violation within the SM. While QED corrections are tiny for fully inclusive observables (when differential in collinear-safe variables), they induce non-universal corrections of the type $(\alpha/\pi) \ln(m_\ell/m_B)$ which can reach the 10% level in the electron mode, when accompanied by tight cuts on the photon energy [4, 5]. These effects are corrected for by the experimental collaborations: the value in Eq. (1.2), as well as the results for the LFU ratios reported in [9, 10], correspond to photon-inclusive observables (in the collinear safe differential variable q_0^2 , cf. Sec. 2.1.) However, what is really measured are not photon-inclusive observables: tight cuts on reconstructed B mass are employed to reduce, amongst the different background contributions, events originated from resonant modes, e.g. $\bar{B} \rightarrow \bar{K}(J/\Psi \rightarrow \ell^+\ell^-)$ that leak into the signal region. The photon-inclusive results are obtained by comparing with appropriate Monte Carlo (MC) simulations. The purpose of this paper is to check this procedure using a dedicated MC-framework developed on grounds on our earlier work [5]. The latter consists of a complete differential description of $O(\alpha)$ QED corrections in $\bar{B} \rightarrow \bar{K}\ell^+\ell^-(\gamma)$ based on an effective meson theory.

In the experimental analyses, QED corrections are implemented via photon shower algorithms such as PHOTOS [11–14], or the PHOTONS++ module [15] of SHERPA [16], where mesons are treated as point-like particles. In [5], using gauge invariance, it was shown that no further lepton non-universal collinear logs (i.e. $\ln(m_\ell)$ terms) are generated by structure dependent corrections, i.e. that the point-like approximation for the mesons is a very good approximation, especially when considering LFU ratios. The photon shower algorithms used by the experiments therefore do provide a very good starting point to describe data. In practice, QED corrections in $\bar{B} \rightarrow \bar{K}\ell^+\ell^-(\gamma)$ are not treated perfectly due to the resonant mode being simulated separately from the rare mode, therefore neglecting the respective interference. The latter is a potentially dangerous effect due to the *migration* towards lower q^2 -values of events with on-shell charmonium resonances and sizeable photon-energy emission: an effect which is particularly pronounced for the electron mode [4, 5].

This paper consists of two parts. Firstly, the description of our MC-framework based on [5], and its comparison with PHOTOS at the fully differential level, considering the rare mode only (i.e. the short-distance (SD) part of the decay amplitude) is discussed. Second, going beyond the PHOTOS analysis, we assess the impact of the charmonium resonances (or the long-distance (LD) contribution to the decay amplitude), which is particularly relevant in the electron mode [6–8]. This second part is addressed in a twofold manner: i) by means of our MC-framework, assessing the impact of the SD–LD interference effects

(not included in PHOTOS), focusing on the region $q^2 \in [1.1, 6] \text{ GeV}^2$; ii) by means of a semi-analytic approach, using the splitting function, assessing the complete impact of the resonant modes beyond interference terms (and resumming the leading collinear logs).

We limit our analysis to the neutral mode $\bar{B}^0 \rightarrow \bar{K}^0 \ell^+ \ell^-$. This choice does not limit the validity of our conclusions on SD–LD interference effects due to charmonium resonances, whilst it has an important simplification for the numerical study. In this case, we can analyse in full generality the impact of the hadronic form factor, without resorting to a derivative expansion in the underlying meson effective theory [5].

It is noted that a first comparison of analytical estimates of QED corrections and PHOTOS has been presented in Ref. [4]. The present study provides significant improvements compared to [4] on various aspects: i) building a dedicated MC to simulate $\bar{B} \rightarrow \bar{K} \ell^+ \ell^- (\gamma)$ events, we are able to perform an extensive study of the tool used to interpret data at a fully differential level; ii) our MC is valid for generic photon kinematics, while the analysis of [4] implicitly assumed tight cuts on the photon-angle emission (cf. App. A.2 [5]); iii) we perform a detailed study of the effects of the resonances, taking into account also the variation of the strong phase between SD and LD contributions.¹

The paper is organised as follows. In Sec. 2, we introduce the the basic kinematics of the process and the principles of our MC-approach. In the following Sec. 3, we compare kinematic distributions obtained with our MC-simulation with those obtained with PHOTOS. The impact of charmonium resonances is discussed in Sec. 4. Finally, in Sec. 5, we summarise our results and present a brief outlook. Technical details are deferred to Apps. A, B to D and supplementary plots are collected in App. C.

2. Monte Carlo Framework

2.1. Generalities

The process of interest is

$$\bar{B}(p_B) \rightarrow \bar{K}(p_K) \ell_1(\ell_1) \bar{\ell}_2(\ell_2) + \gamma(k) . \quad (2.1)$$

In the absence of photon emission, it is a 3-body process, while in the presence of real photon emission, it corresponds to a 4-body process. The latter is characterised by five independent kinematic variables, cf. App. A. The two kinematic variables adopted to describe the 3-body kinematics, or even the 4-body one if the photon is not detected, are

$$q^2 = (\ell_1 + \ell_2)^2 \quad \text{and} \quad c_\ell \equiv \cos \theta_\ell = - \left(\frac{\vec{\ell}_1 \cdot \vec{p}_K}{|\vec{\ell}_1| |\vec{p}_K|} \right)_{q\text{-RF}} , \quad (2.2)$$

where q -RF denotes the dilepton rest frame (RF). If the B momentum is known (e.g. at the generator level, or in a B -factory type experimental setup) the following the kinematic variables

$$q_0^2 = (p_B - p_K)^2 \quad \text{and} \quad c_0 \equiv \cos \theta_0 = - \left(\frac{\vec{\ell}_1 \cdot \vec{p}_K}{|\vec{\ell}_1| |\vec{p}_K|} \right)_{q_0\text{-RF}} , \quad (2.3)$$

¹ Some other studies related to Monte Carlo are for semileptonic modes $B \rightarrow \pi \ell \nu$ [17] and $B \rightarrow D \ell \nu$ [18] and are different in that they do not contain resonances from the phenomenological viewpoint alone.

are more useful [5]. Furthermore we define

$$\bar{p}_B \equiv p_B - k = \ell_1 + \ell_2 + p_K, \quad \bar{p}_B^2 = (m_B^{\text{rec}})^2, \quad (2.4)$$

which corresponds to the reconstructed B -meson mass from its visible decay products, and the variable δ_{ex} ,

$$(m_B^{\text{rec}})^2 = m_B^2(1 - \delta_{\text{ex}}), \quad 0 < \delta_{\text{ex}} < 1, \quad (2.5)$$

which provides a natural choice for the physical cut-off regulating soft divergences of real photons emission.

As stated in many textbooks, a photon energy cut-off, m_B^{rec} or δ_{ex} in our case, is sufficient to define IR-safe observables (for massive charged particles). However, this is not the procedure applied in many of today's experiments, especially at hadron colliders. In this case the event distributions are *fitted* in a given window of $m_B^{\text{rec}} > m_B^{\text{rec},\ell}$ and m_B^{rec} becomes a key differential variable. Using the simulated shape in m_B^{rec} , by a MC-tool (e.g. PHOTOS), the theoretical non-radiative rate in the IR-safe differential variable q_0^2 is reconstructed.² Checking the validity of this procedure requires the comparison of the MC-tool used in the data analysis with one based on a QED calculation defined in a full theoretical framework, such as the one presented in [5]. The validation of the procedure ensures that, within the SM, the measured R_K is then $R_K|_{\text{reconstr.}}^{\text{SM}} = 1 + \mathcal{O}(\frac{\alpha}{\pi})$, where $\alpha = e^2/(4\pi) \approx 1/137$ is the fine structure constant.

2.2. Basic strategy of the Monte Carlo approach

The strategy of our MC-framework is based on the following steps:

- We introduce a technical cut-off $E_{\gamma,\text{cut}}^{(i)}$ on the photon energy in a given RF (indicated by the superscript i). This cut-off is chosen well below the experimental resolution on the missing energy, such that events with $E_\gamma^{(i)} < E_{\gamma,\text{cut}}^{(i)}$ can be simulated according to 3-body kinematics, while events with $E_\gamma^{(i)} > E_{\gamma,\text{cut}}^{(i)}$ are simulated according to 4-body kinematics.
- The 3-body and 4-body events are simulated according to the corresponding (Born-level) distributions reported in Ref. [5], which depends on the $f_\pm(q^2)$ hadronic form factors for $B \rightarrow K$. The relative normalisation between 3-body events (N_3) and 4-body events (N_4), namely the ratio

$$f^{\text{th}} \equiv \frac{N_3}{N_4} \equiv \frac{\Gamma_3}{\Gamma_4} = f(E_{\gamma,\text{cut}}^{(i)}), \quad (2.6)$$

is the key theory input for the numerical simulation.

- The 3-body rate is computed at $\mathcal{O}(\alpha)$, taking into account both virtual and real corrections. By construction, Γ_3 is free from soft divergences, but it depends logarithmically on the (artificial) photon energy cut-off $E_{\gamma,\text{cut}}^{(i)}$. It can be decomposed

²In terms of the q_0^2 -variable, the single-differential non-radiative rate is equivalent to the fully photon-inclusive rate up to $\mathcal{O}(\frac{\alpha}{\pi})$ corrections.

as

$$\Gamma_3 = \Gamma_{\text{soft-log}} \ln E_{\gamma, \text{cut}}^{(i)} + \Gamma_{\text{rest}}^{(i)} . \quad (2.7)$$

Here, $\Gamma_{\text{soft-log}}$ is the well-known universal (Lorentz-invariant) coefficient of the soft singularities [19], while $\Gamma_{\text{rest}}^{(i)}$ is a frame-dependent quantity, indicated by the superscript [5].

- A key simplification for the determination of f^{th} is the observation that the total rate Γ_{tot} is equal to the tree-level rate, Γ_{tree} , up to finite (non-log enhanced) corrections of $\mathcal{O}(\alpha)$:

$$\Gamma_{\text{tot}} \equiv \Gamma_3 + \Gamma_4 = \Gamma_{\text{tree}} \times [1 + \mathcal{O}(\alpha)] . \quad (2.8)$$

Neglecting the tiny $\mathcal{O}(\alpha)$ terms, this allows us to extract f^{th} simply by the ratio $\Gamma_{\text{tree}}/\Gamma_3$, via the relation

$$f^{\text{th}} = \left(\frac{\Gamma_{\text{tree}}}{\Gamma_3} - 1 \right)^{-1} . \quad (2.9)$$

- As demonstrated in [5], the q_0^2 single-differential spectrum is also free from soft and collinear divergences. This implies that the relation (2.8) holds not only for the total rate, but also for the q_0^2 single-differential rate (or partial rates defined on a given q_0^2 interval). Using Eq. (2.9) simplifies the numerical analysis considerably, since $\Gamma_{\text{tree}}/\Gamma_3$ can be determined using only 3-body phase-space integrations. The values of $\Gamma_{\text{tree}}/\Gamma_3$ computed using the analytic code from [5] relevant to the present study are reported in Tab. 3 in App. D.

2.3. Numerical procedure

The 3- and 4-body decay rates are implemented in a numerical framework by means of the `zfit` package [20]. They are interpreted as (non-negative) probability distribution functions (PDFs) with an a priori unknown normalisation. This allows us to generate the MC samples by means of the hit-or-miss algorithm. The concrete sampling procedure, for both 3- and 4-body decays, is outlined as follows:

1. A single point in phase space, denoted by \vec{x} , is uniformly sampled in the kinematically allowed region of (q^2, c_ℓ) or $(q^2, \vec{p}_B^2, c_\ell, c_\gamma, \phi_\gamma)$ for simulated 3- or 4-body events, respectively.
2. Using the kinematic decomposition reported in App. A, the sampled variables are translated to the corresponding momenta of the B decay products. The scalar products that enter the decay widths, as well as the decay width $\Gamma(\vec{x})$ itself, are evaluated at the sampled point in phase space.
3. A random number r is extracted uniformly in the range $r \in [0, m]$, where m is the maximum value of the decay width in the allowed kinematic range. If $r > \Gamma(\vec{x})$ (“miss”) points 1. and 2. are repeated until for one sampled r , $r < \Gamma(\vec{x})$ (“hit”) and the point \vec{x} is kept.

The standard hit-or-miss algorithm can suffer from very low sampling efficiency in the case where the decay width exhibits pronounced peaks since it only accepts a fraction of extractions equal to the ratio of the volume under $\Gamma(\vec{x})$ and the volume of the hypercube containing $\Gamma(\vec{x})$ itself. This is valid in particular for the 4-body decay width $\Gamma_4(\vec{x})$ which is peaked close to collinear and soft regions. In order to increase the sampling efficiency, the ‘‘importance sampling’’ technique is employed. This technique consists in dividing the support, over which \vec{x} is sampled, such that in each subinterval, $\Gamma(\vec{x})$ has a smaller variation than in the overall range, hence allowing to increase the sampling efficiency by one to two orders of magnitude.

We compare our MC-approach against the EvtGen [21] + PHOTOS [11, 12] which are the simulation software packages used by the LHCb collaboration. The former is an event generator specifically designed for B -physics in which the decay amplitudes (models), instead of PDFs, are used for the simulation of heavy meson decays. PHOTOS encodes the QED radiative corrections to such decays and uses a splitting function approach iteratively. In principle, this achieves the inclusion of the leading logs and thus, remaining discrepancies can be expected to be of $\mathcal{O}(\frac{\alpha}{\pi})$. Since 2005, when multi-photon radiation was introduced [13], there were no further public upgrades of the program until 2010, when PHOTOS was moved to a C++ environment allowing the use of event records such as HepMC [22]. We employ version 3.64 which enables the use of PHOTOS in the case where there are no parent particle(s) or incoming beams generating the decaying particle, which, paired with the EvtGen package, allows us for a direct comparison with our MC simulation. In order to match the EvtGen model with our description of the decay, $\mathcal{O}(\alpha_s)$ two-loop virtual corrections [23] to the decay width are switched off from the default EvtGen configuration.

Moreover, since our MC accounts for QED corrections up to $\mathcal{O}(\alpha)$, for each B decay in which more than a real photon is emitted, only the hardest emission is considered and all the softer emissions’ momenta are summed and saved into one ‘‘particle’’ for further cross-checks.

3. Direct Comparison with PHOTOS at the Short Distance Level

3.1. Parameterisation of the short distance amplitude

In this section, we compare our MC-method, as described in Sec. 2.3, with the PHOTOS framework at the level of the SD contribution. Since both frameworks are expected to capture the leading logs one should expect differences to be of order of $\mathcal{O}(\frac{\alpha}{\pi})$ only. Let us first define the SD amplitude. Following our previous conventions [5], we write

$$\mathcal{A}_{\bar{B} \rightarrow \bar{K} \ell^+ \ell^-} \equiv \langle \bar{K} \ell^+ \ell^- | (-\mathcal{L}_{\text{int}}) | \bar{B} \rangle = \frac{G_F}{\sqrt{2}} V_{ts}^* V_{tb} L_0 \cdot H_0 + \mathcal{O}(\alpha), \quad (3.1)$$

where L_0 and H_0 correspond to the leptonic and hadronic parts which read

$$\begin{aligned} L_0^\mu(q^2) &= \bar{u}(\ell^-) \gamma^\mu (C_V + C_A \gamma_5) v(\ell^+), \\ H_0^\mu(q^2) &= f_+(q^2) (p_B + p_K)^\mu + f_-(q^2) (p_B - p_K)^\mu, \end{aligned} \quad (3.2)$$

with $C_{V(A)} = -\alpha C_{9(10)}/(2\pi)$, thereby neglecting the dipole operator O_7 as justified for a scalar meson final state.³ The SD contribution consists of the standard form factors f_{\pm} . Note that when f_- is traded for the scalar form factor $f_0 = f_+ + \frac{q^2}{m_B^2 - m_K^2} f_-$ only f_+ enters the vector part $C_V \propto C_9$. The specific form factors are taken from [24] (with set 2), which is a light-cone sum rules computation up to NLO twist-3 and $\mathcal{O}(\alpha_s)$, and is also used by the LHCb collaboration.

3.2. Comparison of our Monte Carlo with PHOTOS

The main results of this section consist of the plots in Fig. 1 and Fig. 2, for the kinematic variables q_0^2 (2.3) and q^2 (2.2), respectively. In each of these figures, the top plots display the impact of the radiative corrections on the q_0^2 - and q^2 -spectra when considering either muons (left) and electrons (right), in our MC. The normalisation per se of the MC-plots is not meaningful as both LO and NLO are separately normalised to 1 when integrated over q_0^2 or q^2 (compare with the normalised plots in Fig. 4 in [5]). This ambiguity can be removed by taking double ratios between our MC-approach and the PHOTOS software as shown in the middle and bottom of these figures for muons and electrons respectively.

Let us discuss the q_0^2 -variable first. Even though the hard-collinear logs cancel in this variable, the introduction of a photon energy cut-off, via $m_B^{\text{rec}} = (4.88, 5.18)$ GeV, leads to sizeable QED contributions. The agreement between the two approaches is excellent as shown by the good compatibility of these distributions with unity across the q_0^2 -spectrum, for both lepton flavours (bottom plot).

The distributions in the q^2 -variable, shown in Fig. 2, are more delicate as hard collinear logs do not cancel. In addition, events can migrate in the q^2 -spectrum due to radiation which will be important when discussing the impact of the resonances. Hence, even without placing a photon-energy cut-off, the corrections are sizeable, cf. Fig. 4 in [5].

Again, the agreement between the two approaches is excellent, as expected, except for electrons at high q^2 where deviations up to $\mathcal{O}(4\%)$ are found. This originates from large corrections that go beyond the fixed $\mathcal{O}(\alpha)$ accuracy of our MC. In fact, at the kinematic endpoint, the corrections are roughly 20% (cf. Fig. 8 in [5]) at NLO, indicating the need of NNLO accuracy to reach % level precision, and explaining qualitatively the residual difference with PHOTOS (where the resummation of the leading-log corrections is implemented). Using the splitting function formalism in Sec. 4.3, in its resummed form, we were able to reproduce quantitatively the $\mathcal{O}(4\%)$ -effect between our MC and PHOTOS (cf. footnote 8).

It is worthwhile to elaborate on why the corrections are large at the kinematic endpoint in q^2 . This happens because, at the endpoint, the leptons carry all the energy and there is effectively no phase space for the real radiation. As a result, near the endpoint in q^2 , virtual corrections dominate and the cancellation between real and virtual corrections is maximally out of balance. In other words, requiring large q^2 is equivalent to a tight cut on the photon emission energy. In the splitting function approach, this can be seen from the

³ In the relation of $C_{V(A)}$ and $C_{9(10)}$ we correct a factor minus two w.r.t. the published version of [5] which, however, has no impact on the result of that paper as all results are relative.

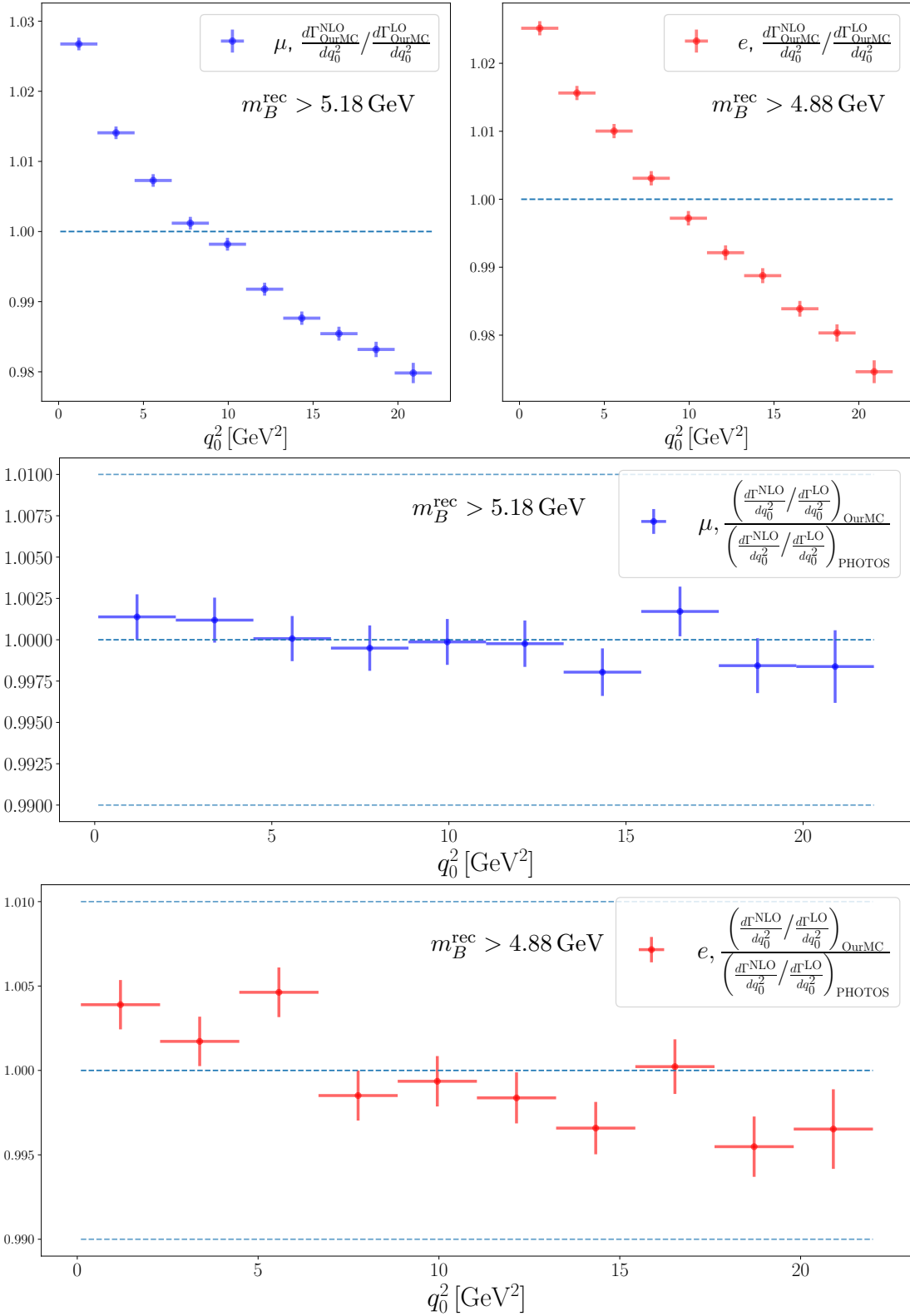


Figure 1. Differential distributions in q_0^2 for the short distance transition only: NLO over LO for muons in blue (top left) and for electrons in red (top right) in our MC, with appropriate cuts as in Tab. 1. The normalisation of these upper plots is arbitrary (cf. main text). The double ratios of our MC versus the PHOTOS framework, shown in the middle and bottom plots, are free of ambiguities.

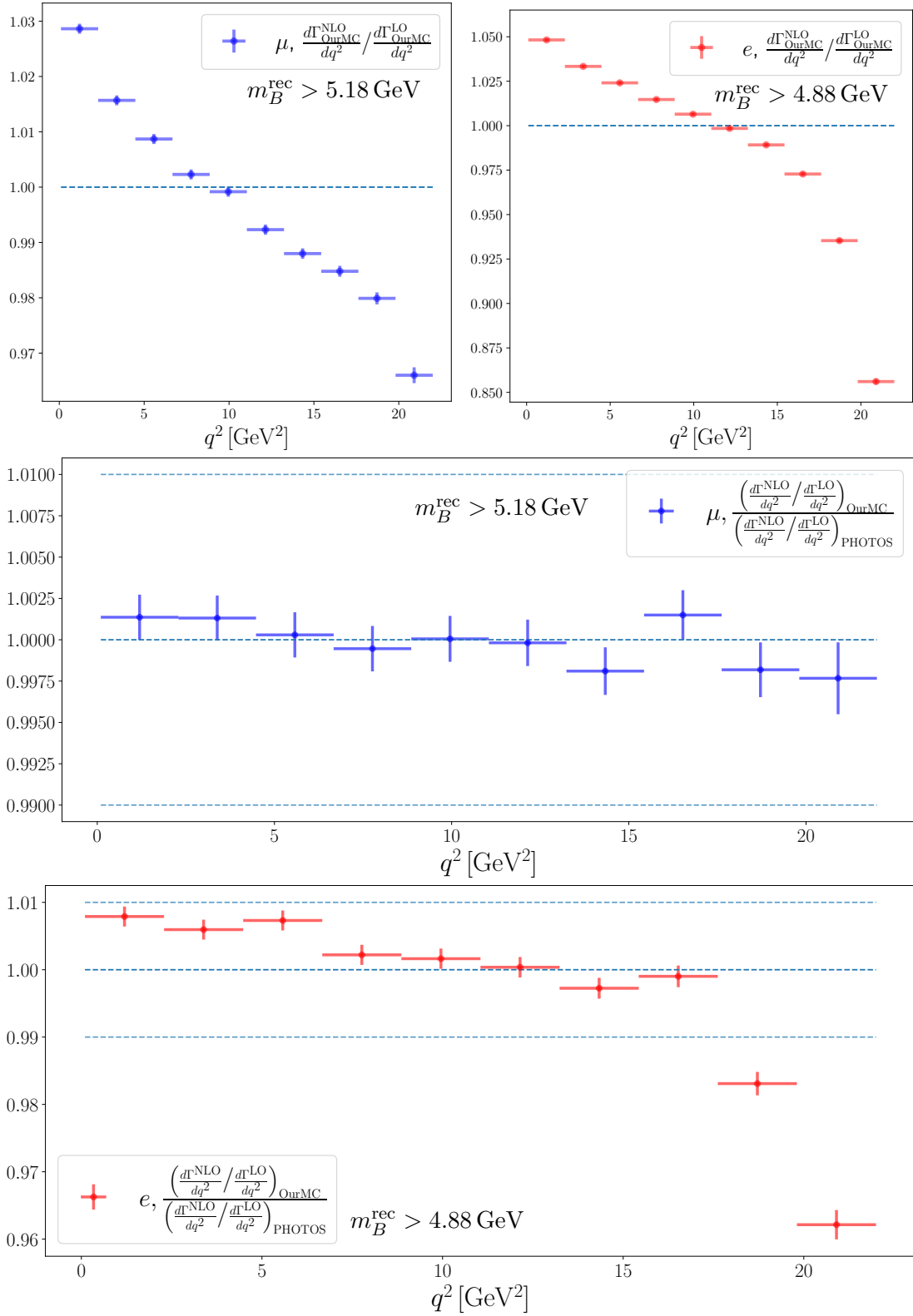


Figure 2. Differential distributions in q^2 for the short distance transition only: The notation is the same as in Fig. 1.

ℓ	$m_B^{\text{rec}} [\text{GeV}]$	δ_{ex}	$(q_0^2)_{\text{max}}$
μ	5.18	0.0486	$q^2 + 1.36 \text{ GeV}^2$
e	4.88	0.146	$q^2 + 4.07 \text{ GeV}^2$

Table 1. Relation between the cut on the reconstructed mass m_B^{rec} and the maximal value of q_0^2 affecting the spectrum at a given q^2 -value, after photon radiation, according to (4.1). The specific values of m_B^{rec} are fixed to the same values used in the LHCb analysis of R_K [25].

lower boundary of the real emission integral (over the momentum fraction carried by the lepton, z) approaching the upper boundary.

In summary, the cross checks we have performed allow us to validate that the approximations adopted by PHOTOS in describing (real and virtual) QED corrections in $\bar{B}^0 \rightarrow \bar{K}^0 \ell^+ \ell^-$ decays are accurate to sub-percent level. Additional plots displaying comparisons of the impact of radiative corrections on the kinematic variable c_ℓ between our MC and PHOTOS can be found in App. C.

4. Adding Long Distance (Charmonium Resonances)

In this section, we assess the impact of the charmonium resonances on the lower part of the spectrum, specifically on the $1.1 \text{ GeV}^2 < q^2 < 6 \text{ GeV}^2$ region currently used to measure the LFU ratios. While the main contribution (peak) of the resonances is cut in the experimental analyses, a residual effect from the radiative tail of the resonances is potentially present at hadron colliders, where the q_0^2 variable is not accessible. As previously mentioned, the migration in q^2 , due to QED radiation, implies that events generated at high q_0^2 (e.g. close to the resonance region) necessarily move down toward low q^2 -values, possibly affecting the *signal* region for the rare mode. The migration is controlled by the m_B^{rec} cut: only events with

$$q^2 \leq q_0^2 \leq (q_0^2)_{\text{max}} \equiv q^2 + \delta_{\text{ex}} m_B^2, \quad (4.1)$$

are relevant to determine radiative corrections at a given q^2 -value.⁴

The m_B^{rec} cuts used to define the signal windows for electron and muon modes in the LHCb analyses are reported in Tab. 1. Note that the cut on the electrons is looser than the one on the muons: a measure implemented to decrease the loss of events in the electron case where radiation effect is stronger. As can easily be checked, in the electron case, events at $q^2 = 6 \text{ GeV}^2$ probe (via photon radiation) the non-radiative spectrum above the J/Ψ -resonance ($m_{J/\Psi}^2 \approx 9.58 \text{ GeV}^2$), but do not probe the $\Psi(2S)$ peak.

This effect is well known and the residual contribution of radiation from the J/Ψ in the signal region is taken into account in the experimental analyses. However, this is simulated as a completely incoherent process, while in reality interference effects between the SD

⁴ The value $(q_0^2)_{\text{max}}$ is reached for photons emitted backward with respect to \vec{q} in the B rest frame [5].

Ψ	m_Ψ [MeV]	$\mathcal{B}(\Psi \rightarrow e^+e^-)$	$\mathcal{B}(\Psi \rightarrow \mu^+\mu^-)$	Γ_Ψ [MeV]
$J/\Psi(1S)$	3097	$5.971(32) \cdot 10^{-2}$	$5.961(33) \cdot 10^{-2}$	92.6(17)
$\Psi(2S)$	3686.1(6)	$7.93(17) \cdot 10^{-3}$	$8.0(6) \cdot 10^{-3}$	294(8)

Table 2. Data of charmonium resonances included in our analysis as taken from [26]. The J/Ψ mass uncertainty is negligibly small.

amplitude and LD one are present. The purpose of this section is to estimate the possible impact of these effects. In Sec. 4.1, we discuss how the amplitude of the rare mode can be adapted to describe SD-LD interference terms. Using this modified parametrisation of the amplitude, in Sec. 4.2, we analyse the numerical impact of the interference terms in our MC-framework. Finally, in Sec. 4.3 we analyse the effect of interference terms, as well as the whole modulus square of the LD amplitude, via a semi-analytic approach.

4.1. Parameterisation of the charm amplitude

We extend the parameterisation of the amplitude in Sec. 3 for the SD form factor by including the effects of the charmonium resonances which we label as long distance (LD)

$$\mathcal{A}_{\bar{B} \rightarrow \bar{K} \ell^+ \ell^-}^{\text{tot}} = \mathcal{A}_{\bar{B} \rightarrow \bar{K} \ell^+ \ell^-}^{\text{SD}} + \mathcal{A}_{\bar{B} \rightarrow \bar{K} \ell^+ \ell^-}^{\text{LD}}. \quad (4.2)$$

The LD contribution can be absorbed into,

$$C_9^{\text{eff}}(q^2) = C_9 + \Delta C_9(q^2), \quad (4.3)$$

a q^2 -dependent Wilson coefficient $\Delta C_9(q^2)$ (recall $C_V \propto C_9$). Its q^2 -dependence is parameterised by an n -times subtracted dispersion relation

$$\Delta C_9(q^2) = \sum_{k \geq 0}^{n-1} \frac{(q^2 - s_0)^k}{k!} \Delta C_9^{(k)}(s_0) + \frac{(q^2 - s_0)^n}{2\pi i} \int_{\text{cut}}^{\infty} \frac{ds}{(s - s_0)^n} \frac{\text{disc}[\Delta C_9](s)}{s - q^2 - i0}, \quad (4.4)$$

with a cut starting just below $m_{J/\Psi}^2$. Above, “disc” stands for the discontinuity, the k -superscript denotes the k^{th} derivative, and “cut” stands for the branch cut. Formally, $n \geq 1$ as otherwise, the dispersion integral is not convergent. In this form, (4.4) is valid in full generality and one can equally write it for the amplitude. For the representation (4.4), the main idea is to evaluate the Taylor series in ΔC_9 for some $q^2 = s_0$, where perturbative methods can be trusted. The discontinuity, $\text{disc}[\Delta C_9]$, which enters the dispersion integral, is approximated by the Breit-Wigner form for the resonances. This is sufficient for the purposes of estimating the contamination of the resonances on $\bar{B} \rightarrow \bar{K} \ell^+ \ell^-$ due to QED-corrections.⁵ The final form of ΔC_9 used is the one corresponding to one subtraction

$$\Delta C_9(q^2) = \Delta C_9(s_0) - \sum_{r \in \Psi} \left(\frac{q^2 - s_0}{m_r^2 - s_0} \right) \frac{\eta_r e^{i\delta_r} m_r \Gamma_r}{q^2 - m_r^2 + i m_r \Gamma_r}. \quad (4.5)$$

⁵ Refinements include the interference of broad resonances [27] and the inclusion of two-particle thresholds assuming strong constant phases [28].

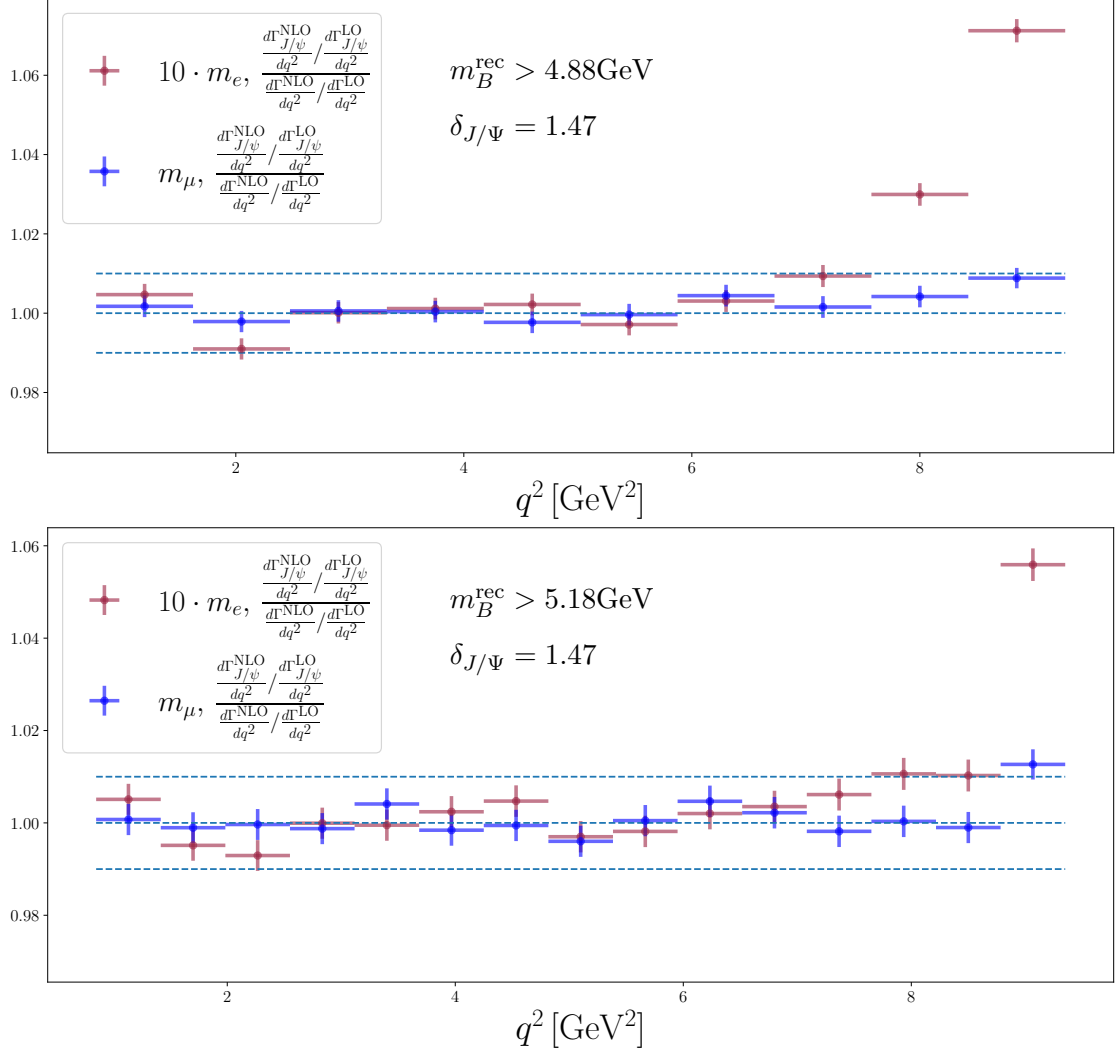


Figure 3. Double ratio of the q^2 -spectrum, with and without the inclusion of interference effects induced by the J/Ψ -resonance, for electron and muons, using the respective reference m_B^{rec} cuts in Tab. 1. For numerical stability we use $m_e \rightarrow 10m_e$ (as indicated by the darker shade in red). The phase of the J/Ψ amplitude, relative to the SD term, is set to $\delta_{J/\Psi} = 1.47$.

The values of the phenomenological coefficients η_r and δ_r for the first two narrow resonances are reported in Sec. 4.2 and Sec. 4.3 respectively (cf. (B.5) on how η_r relates to underlying parameters). The two values used in the subtraction terms are $\Delta C_9(0 \text{ GeV}^2) \approx 0.27 + 0.073i$ and $\Delta C_9(1 \text{ GeV}^2) \approx 0.24 + 0.031i$ in Secs. 4.2 and Sec. 4.3 respectively. More details on the charm parameterisation are deferred to App. B.

4.2. Study of the J/Ψ -resonance interference term in our Monte Carlo

In the MC-study, we include the J/Ψ -resonance in the sampling method outlined in Sec. 2.3, by extending the definition of $C_9^{\text{eff}}(q^2)$ as detailed in the previous section. The modulus squared of the resonant mode, $\mathcal{A}_{\bar{B} \rightarrow \bar{K}(J/\Psi \rightarrow \ell^+ \ell^-)} \subset \mathcal{A}_{\bar{B} \rightarrow \bar{K} \ell^+ \ell^-}^{\text{LD}}$ in Eq. 4.2, is not included

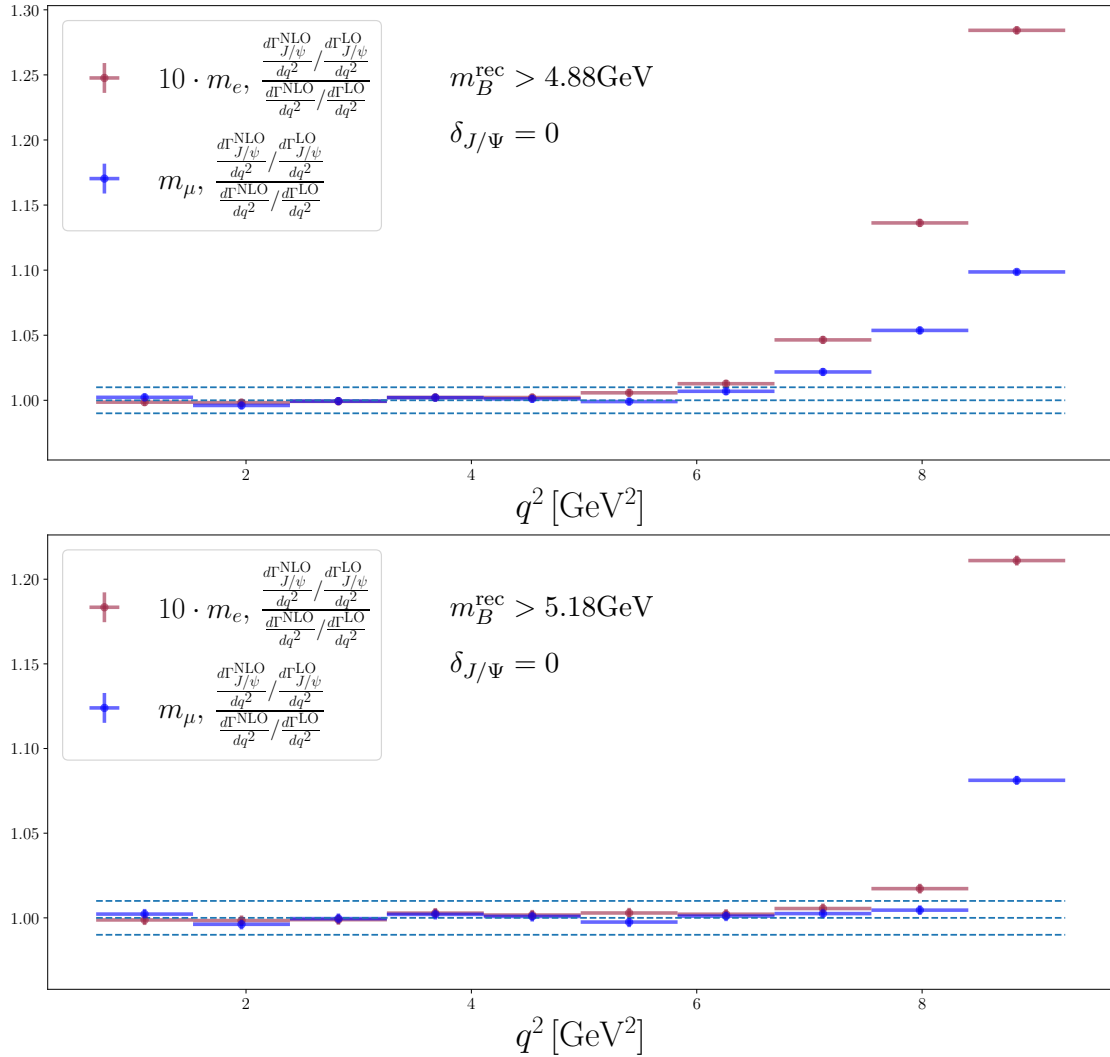


Figure 4. Same plots as in Fig. 3 with the relative phase of the J/Ψ amplitude set to $\delta_{J/\Psi} = 0$.

in our simulation since its sharp pole at $q^2 \approx m_{J/\Psi}^2$ renders the MC sampling efficiency too low. In turn, this requires to place a cut on $q_0^2 \leq 9.59 \text{ GeV}^2$ (cf. App. D for details) since the remaining terms become negative above that threshold, invalidating their interpretation as a PDF (cf. Sec. 2.3). Another factor limiting the sampling efficiency is the lepton mass, which in the electron case has to be increased to 10 times its physical value (c.f. App. D) to allow for efficient sampling.⁶

Our approach is well justified since the modulus squared of the J/Ψ -resonance is well simulated by PHOTOS (see [8]), and the component describing its leakage in the signal region is included in the fit used to extract the rare mode yield. With our simulation, we aim to

⁶ We have checked that the $\ln m_\ell$ -behaviour is consistent with what is obtained using the semi-analytic method described in Sec. 4.3.

analyse the effect on the q^2 bin migration of the J/Ψ interference term, that has so far not been considered in the experimental analyses.

The resonance data is given by the normalisation $\eta_{J/\Psi} = 8180$ in the notation of (4.5) (or $\rho_{J/\Psi} = 1.38$, in the notation of (B.5)), with mass and width in Tab. 2, and the interference phase $\delta_{J/\Psi}$. For the latter, we choose two representative values: $\delta_{J/\Psi} = (1.47, 0)$ where the former is deduced by the LHCb analysis of the dilepton spectrum [29], and the latter is a conservative choice aimed at maximising the J/Ψ interference effect.

The plots in Figs. 3 and 4 show the effect, as a function of q^2 , on the radiative corrections when including the J/Ψ interference term in the decay width, for interference phases of $\delta_{J/\Psi} = (1.47, 0)$ respectively. More specifically, they represent the double ratio of NLO over LO differential decay widths including charm over the same ratio without charm.

Both figures include electron-like (red) and muon (blue) distributions, with appropriate $m_B^{\text{rec}} = (4.88, 5.18)$ GeV cuts (cf. Tab. 1). As can be seen from these plots, the impact of the SD–LD interference term is well below the 1%-level in the $q^2 < 6 \text{ GeV}^2$ region, for the (realistic) phase choice $\delta_{J/\Psi} = 1.47$. Even, in the conservative case $\delta_{J/\Psi} = 0$, it remains just below 1%. We thus conclude that when applying the aforementioned cuts, the experimental approach of neglecting the *interference* effect of charmonium resonances, when fitting for the rare mode in the $q^2 < 6 \text{ GeV}^2$ region, is well-justified.

4.3. J/Ψ and $\Psi(2S)$, including the resonant mode via a semi-analytic approach

Here, we follow a semi-analytic approach, using the splitting function, which reproduces the relevant collinear logarithms. There are a few advantages to this approach: it is numerically less demanding, there is no normalisation ambiguity, no issues with positivity, further resonances are easily incorporated, we can simulate for the actual electron mass and we may assess the impact of the full resonant amplitude. On the other hand, this is not a MC-based approach and cannot be directly used for the actual event simulation.

Evaluating the impact of the full resonant amplitude is of interest since its rate is sizeable $\mathcal{B}(\bar{B}^0 \rightarrow \bar{K}^0 J/\psi) = 8.91(21) \cdot 10^{-4}$ compared to the rare mode itself which is $\mathcal{O}(10^{-6})$, and with a cut set at $m_B^{\text{rec}} = 4.88 \text{ GeV}$ the electron mode does probe the first resonant peak for $q^2 \approx 6 \text{ GeV}^2$, as previously stated. In fact, in a decay like $\bar{B} \rightarrow \bar{K} \ell^+ \ell^-$ the collinear and soft-collinear logs in the lepton mass can be reproduced from the lepton to lepton-photon splitting function.^{7,8}

It is convenient to parameterise the relative QED correction $d^2\Gamma \propto (1 + \Delta^{(\ell)}(\hat{q}^2, c_\ell)) d\hat{q}^2 dc_\ell$, following our earlier work, as

$$\Delta_{\text{hc}}^{(\ell)}(\hat{q}^2, c_\ell) = \frac{\alpha}{\pi} \left(\frac{1}{\Gamma^{\text{LO}}} \frac{d^2\Gamma^{\text{LO}}(\hat{q}^2)}{d\hat{q}^2 dc_\ell^2} \right)^{-1} (\hat{Q}_{\ell_1}^2 \tilde{\Delta}_{\text{hc}, \ell_1}^{(\ell)} + \hat{Q}_{\ell_2}^2 \tilde{\Delta}_{\text{hc}, \ell_2}^{(\ell)}). \quad (4.6)$$

⁷ The specific details are postponed to a future publication [30] and for more generic remarks we refer the reader to [31]. Although, note that the kinematic relations, to follow below, can be found in our previous work [5] (cf. ancillary notebook for the expression with $m_K \neq 0$). Eq. (A.5) in [5] corresponds to the single-differential and photon-inclusive version of (4.7).

⁸ This formalism can be extended to resum all the collinear logs using the electron structure function. Taking the last bin $[20.9 \text{ GeV}^2, (m_B - m_K)^2]$, used in Fig. 2, and weighing by the rate, we produce an effect of ≈ 0.96 which agrees very well with the central value in that figure.

where $\hat{q}^2 \equiv q^2/m_B^2$ for brevity and the subscript “hc” stands for the (hard) collinear contribution. This quantity reads

$$\tilde{\Delta}_{\text{hc}, \ell_1}^{(\ell)}(\hat{q}^2, c_\ell) = \ln \frac{\mu_{\text{hc}}}{m_{\ell_1}} \left(\frac{1}{\Gamma^{\text{LO}}} \int_{\max(\hat{q}^2, z_{\ell_1}^{\delta})}^1 dz P_{f \rightarrow f\gamma}(z) \frac{d^2 \Gamma^{\text{LO}}(\hat{q}_0^2, c_0)}{d\hat{q}_0^2 dc_0} \right) J_{\ell_1}(c_\ell, z), \quad (4.7)$$

where the splitting function is $P_{f \rightarrow f\gamma}(z) = \frac{1+z^2}{(1-z)_+} + \frac{3}{2}\delta(1-z)$ with $\frac{1}{(1-z)_+}$ being the standard plus regularisation and $\mu_{\text{hc}} = \mathcal{O}(m_B)$ is an a priori undetermined scale (to be commented further below). The variable relations and the Jacobian ($dq_0^2 dc_0 = J_{\ell_1}(c_\ell, z) dq^2 dc_\ell$) are given by

$$q^2 = zq_0^2, \quad c_0|_{m_K=0} = \frac{c_\ell(1+z) + \bar{z}}{c_\ell \bar{z} + 1 + z}, \quad J_{\ell_1}(c_\ell, z)|_{m_K=0} = \frac{4}{(c_\ell \bar{z} + 1 + z)^2}, \quad (4.8)$$

with $\bar{z} \equiv 1 - z$. The lower integration boundary is set by the maximum of the photon inclusive limit \hat{q}^2 and the photon-cut off dependent

$$z_{\ell_1}^{\delta}|_{m_K=0} = \frac{1 + \hat{q}^2 - \delta + c_\ell(1 - \hat{q}^2 - \delta)}{1 + \hat{q}^2 + \delta + c_\ell(1 - \hat{q}^2 - \delta)}. \quad (4.9)$$

The corresponding expression for $\tilde{\Delta}_{\text{hc}, \ell_2}^{(\ell)}$ can be obtained by changing the signs on all the cosines in the lepton angles in Eqs. (4.8) and (4.9).

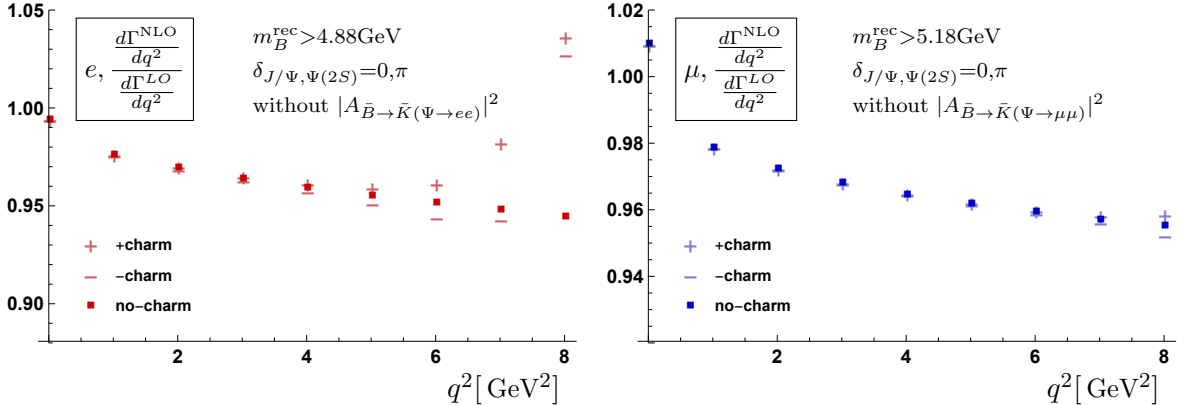


Figure 5. Plots with the resonant mode cut out (cf. main text for explanation). For $q^2 < 6 \text{ GeV}^2$ the interference effects are small, even in the electron case (confirming the plot in Fig. 4), and do not indicate any contamination to R_K in particular. The corresponding plot without the LO normalisation can be found in App. C in Fig. 8.

We turn to the practical implementation. As compared to the previous section, we include the second resonance $\Psi(2S)$, cf. Tab. 2 for the basic inputs. In this case $\eta_{\Psi(2S)} = 1160$ (or $\rho_{\Psi(2S)} = 1.56$, in the notation of (B.5)) describes its residue up the free phase $\delta_{\Psi(2S)}$. In order to emulate the LHCb procedure in eliminating the J/Ψ mode, we cut out the amplitude squared of the resonant mode in the following q_0^2 -window: $m_\Psi^2 - \Delta\omega^2 < q_0^2 < m_\Psi^2 + \Delta\omega^2$ with $\Delta\omega^2 = 0.1 \text{ GeV}^2$. Empirically, we find that choosing the undetermined scale to be $\mu_{\text{hc}}^2 \approx 6q^2$, does reproduce our short distance results in [5] rather well. It is not

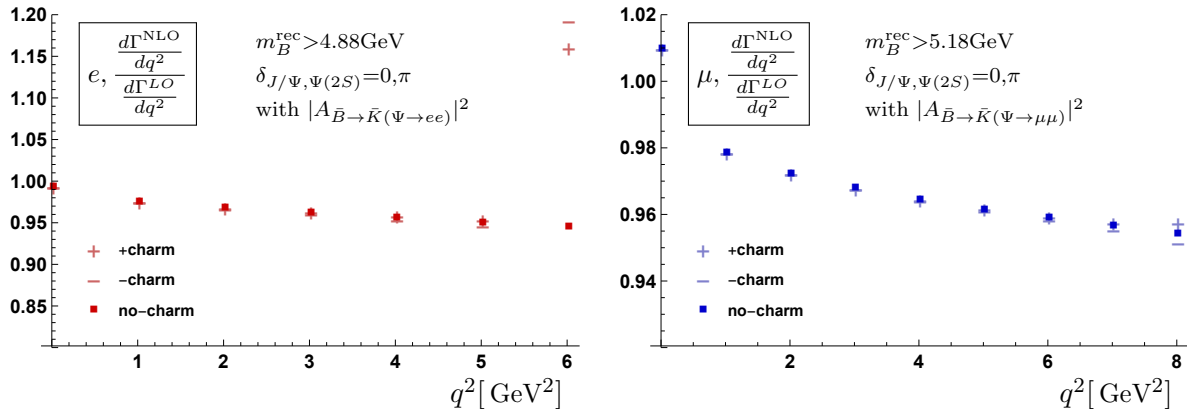


Figure 6. Same plots as in Fig. 5 including resonant modes: (left) for electrons and (right) for muons respectively. It is noted that at $q^2 = 6 \text{ GeV}^2$, the effect is noticeable for electrons and care has to be taken (cf. main text). For the electrons, the plot ends at $q^2 = 6 \text{ GeV}^2$ since beyond this value the effects are too large (at $q^2 = (7, 8) \text{ GeV}^2$ we find, approximately, (6.5, 40) and (8.4, 73) for +charm and -charm respectively). We have checked that resummation slightly tames the effect but qualitatively, it remains the same. The muon plot looks deceptively similar to the one in Fig. 5 for $q^2 < 8 \text{ GeV}^2$ but differences arise thereafter. The corresponding plot without the LO normalisation can be found in App. C in Fig. 9.

surprising that the scale is proportional to q^2 since this is the relevant scale “seen” by the lepton pair.

In order to assess the possible uncertainty of the charm contribution, we choose the phases to give rise to maximal interference i.e. $\delta_{J/\Psi, \Psi(2S)} = 0$ and plot the three graphs: one without any charm, one as described above and one with the sign reversed (i.e. $\delta_{J/\Psi, \Psi(2S)} = \pi$). The maximal difference can then be seen as a conservative estimate for the error of not including the charm.

Plots for the electron and the muon cases with the resonances cut out are shown in Fig. 5. This situation mimics the interference of the rare and resonant mode and it is seen from the plots that, for $q^2 < 6 \text{ GeV}^2$, this contribution is small. At $q^2 = 6 \text{ GeV}^2$ the difference between the two charm contributions with opposite sign is 2% and when this effect is averaged over the entire $[1.1, 6] \text{ GeV}^2$ bin it is clear that the effect does not exceed $\mathcal{O}(1\%)$ which would be comparable to structure dependent corrections. This is fortunate since, as previously mentioned, resonant versus rare-mode interference are not included in the LHCb analysis. These results can be seen as a validation of the double ratio plots in Fig. 4 obtained in the MC-framework (with meaningful absolute normalisation).

We turn to the case where we include the full resonant mode. Crucially, the squared resonant amplitude is independent of the $\delta_{J/\Psi}$ -phase and dominates over the interference. This can be seen from the electron plot shown in Fig. 6, by comparing it to the corresponding one in Fig. 5. Furthermore, it can be seen that for the electron cut-off, QED effects begin to be sizeable below the $q^2 < 6 \text{ GeV}^2$ and thus care has to be taken.

This is further reflected in the LHCb mass fit projections to the signal mode (cf. Fig. 2 in [8]) where the leakage of the resonant mode is included in the total fit model, together

with the other backgrounds components, to extract the electron signal yield. Amongst the cross-checks performed in the measurement of R_K are the integrated and differential ratios $r_{J/\Psi}$, which directly compare electron and muon detection efficiencies, and thus constitute a stringent validation of their analysis. The value of $r_{J/\Psi}$ is known in the SM to be unity to a very high degree of accuracy, since it originates from the tree level mediated resonant mode, and was measured in the R_K analysis, $r_{J/\Psi} = 0.981 \pm 0.020$. This result is one sigma compatible the SM prediction and with the previous measurements of this quantity [26]. Moreover, as can be seen from Fig. 9-10 of [8], $r_{J/\Psi}$ is also performed differentially as a function of variables which are used in the determination of the dilepton invariant mass, such as the opening angle of the lepton pair and their transverse momentum. The flatness of $r_{J/\Psi}$ in those variables reflects an excellent description of the efficiency-related effects in muons and electrons. Not only are these crucial cross-checks per se, but they also validate the double ratio method used to minimise the efficiency-related systematic error in the R_K measurement [8], and the accuracy in the description of the QED corrections from the absolute square of the J/Ψ -mode.

Despite all these positive cross-checks, since the overall impact of the resonance modes is large (cf. Fig. 5), it would be of great relevance if the LHCb collaboration could perform a q^2 -binned analysis of R_K . This would provide a further important test of the robustness of R_K .

Related to that, we have done the analysis with with zero subtractions in (4.4) as opposed to one subtraction (as in Fig. 6). If the hadronic input and the subtraction constant of perturbative QCD were completely consistent, then this would have no impact. However, at $q^2 = 6 \text{ GeV}^2$, in the electron case, a 10%-raise appears for zero versus one subtraction point. At $q^2 = 5 \text{ GeV}^2$ this effect is no longer relevant. That there is an effect does not come as a complete surprise as two resonances are not enough to reproduce the asymptotics of perturbative QCD. All in all, this underlines the importance of a refined q^2 -binning from a different viewpoint. Another way to look at it is that it emphasises the importance of knowing the LO amplitude (i.e. the idealised amplitude in the absence of QED) since its precise form affects the detailed form (size and magnitude) of QED corrections. In this respect, given the smaller impact of QED effects and the better experimental resolution, the muon case can serve as a tool for a precise determination of the LO spectrum in a data-driven approach.

5. Outlook and Conclusions

In this article, we investigated numerical aspects of QED corrections on the $\bar{B}^0 \rightarrow \bar{K}^0 \ell^+ \ell^-$ decay, which is of particular relevance in view of LFU tests. We constructed a dedicated Monte Carlo framework based on the computation in [5] (cf. Sec. 2), and further analysed QED effects by means of a semi-analytic (splitting-function based) approach (cf. Sec. 4.3) which captures the numerically dominant collinear logs.

In Sec. 3, we compared our Monte Carlo framework with PHOTOS at the level of the short distance matrix element (rare mode) and found good agreement at the differential level in all relevant variables (in particular q^2, c_ℓ and q_0^2, c_0). Particularly relevant is the

comparison in the q^2 -distribution, illustrated in Fig. 2, which plays a key role in the LFU tests at hadron colliders. Since PHOTOS and our approach are supposed to capture all the leading logs, agreement was to be expected. Indeed, a partial cross-check of PHOTOS, in the q_0^2 - and with an effective cut-off in the q^2 -distribution were already reported in [4]. Our double differential comparison thus provides a solid cross-validation of both our Monte Carlo framework and PHOTOS.

In addition to the short distance contribution, our Monte Carlo and semi-analytic framework has allowed us to assess the impact of the resonant mode $\bar{B} \rightarrow \bar{K}(J/\Psi \rightarrow \ell^+\ell^-)$ on the extraction of R_K (in Secs. 4.2 and 4.3 respectively). Both the Monte Carlo and the semi-analytic approach confirm that the interference effects between resonant and rare mode (not included in PHOTOS) are below 1% for $q^2 < 6 \text{ GeV}^2$. This justifies not simulating these effects in the experimental setup, as currently done. On the other hand, the resonant mode, as known and expected, has a significant effect in the electron mode below 6 GeV^2 as the plot in Fig. 6 quantifies. This is taken care of in the present experimental analyses. As pointed out, a useful validation of this procedure could be obtained with an extraction of R_K in different q^2 -bins (in the $q^2 < 6 \text{ GeV}^2$ region). A further independent cross-check could be obtained varying m_B^{rec} (in particular setting a tighter cut on the electron mode). Last but not least, we stress that a precise description of the q^2 -dependence of the non-radiative amplitude, including short- and long- distance terms, is a key ingredient to obtain the $\mathcal{O}(\alpha)$ corrections at the sub-percent level (cf. remarks at the end of Sec. 4.3).

In this paper, we have specifically focused on the case of neutral hadrons, which has facilitated the implementation of an arbitrary q^2 -dependence in the form factor. As discussed, we expect the conclusions for the charged modes to be qualitatively similar, especially as far as the interference effects between resonant and rare modes are concerned. Moreover, the same outcomes ought to hold for the $\bar{B} \rightarrow \bar{K}^*\ell^+\ell^-$ and the $\Lambda_b \rightarrow \Lambda\ell^+\ell^-$ modes.

A decisive aspect is that the remaining QED corrections, due to structure dependence, which are not incorporated in PHOTOS, have been shown to be free of $\ln m_\ell$ enhanced factors (cf. Sec. 3.4 [5]). An interesting aspect of charged kaons (or pions) in the final state is that sizeable $\ln m_{K(\pi)}$ -effects can appear in this case. However, they would cancel in LFU ratios [4, 5], along with (other) structure dependent effects, for the reasons mentioned above.

Putting all these ingredients together, the present analysis provides an important further validation that the LFU tests so far performed by the LHCb collaboration are robust with respect to LFU violations induced by QED corrections.

Acknowledgement RZ is supported by an STFC Consolidated Grant, ST/P0000630/1. This project has received funding from the European Research Council (ERC) under the European Union’s Horizon 2020 research and innovation programme under grant agreement 833280 (FLAY), and by the Swiss National Science Foundation (SNF) under contract 200020_204428. This work was supported by the GLUODYNAMICS project funded by the “P2IO LabEx (ANR-10-LABX-0038)” in the framework “Investissements d’Avenir” (ANR-11-IDEX-0003-01) managed by the Agence Nationale de la Recherche (ANR), France.

A. Kinematics

Following Ref. [5], we reproduce the relevant kinematic parameterisation for the 4-body decay kinematics in terms of the five independent variables $(q^2, \bar{p}_B^2, c_\ell, c_\gamma, \phi_\gamma)$, where $c_i \equiv \cos \theta_i$. We start by defining the photon and the meson momenta in the \bar{p}_B -RF (indicated by an upper index (2)):

$$\begin{aligned} k^{(2)} &= (E_\gamma^{(2)}, -\cos \theta_\gamma |\vec{k}_\gamma^{(2)}|, -\sin \theta_\gamma \cos \phi_\gamma |\vec{k}_\gamma^{(2)}|, -\sin \theta_\gamma \sin \phi_\gamma |\vec{k}_\gamma^{(2)}|), \\ \bar{p}_B^{(2)} &= (\bar{p}_B, 0, 0, 0), \quad q^{(2)} = (\bar{p}_B - p_K)^{(2)} = (\bar{p}_B - E_K^{(2)}, |\vec{p}_K^{(2)}|, 0, 0) = (E_q^{(2)}, |\vec{p}_K^{(2)}|, 0, 0), \\ p_K^{(2)} &= (E_K^{(2)}, -|\vec{p}_K^{(2)}|, 0, 0). \end{aligned} \quad (\text{A.1})$$

Here,

$$\begin{aligned} E_K^{(2)} &= \sqrt{|\vec{p}_K^{(2)}|^2 + m_K^2} = \frac{1}{2\bar{p}_B} (\bar{p}_B^2 - q^2 + m_K^2), \quad |\vec{p}_K^{(2)}| = \frac{\lambda^{1/2}(\bar{p}_B^2, q^2, m_K^2)}{2\bar{p}_B}, \\ E_\gamma^{(2)} &= \sqrt{|\vec{k}_\gamma^{(2)}|^2 + m_\gamma^2} = \frac{1}{2\bar{p}_B} (m_B^2 - \bar{p}_B^2 - m_\gamma^2), \quad |\vec{k}_\gamma^{(2)}| = \frac{\lambda^{1/2}(\bar{p}_B^2, m_B^2, m_\gamma^2)}{2\bar{p}_B}, \\ E_q^{(2)} &= \sqrt{|\vec{p}_K^{(2)}|^2 + q^2} = \frac{1}{2\bar{p}_B} (\bar{p}_B^2 + q^2 - m_K^2), \end{aligned} \quad (\text{A.2})$$

and

$$\lambda(s, m_1^2, m_2^2) = (s - (m_1 - m_2)^2)(s - (m_1 + m_2)^2). \quad (\text{A.3})$$

The lepton momenta $\ell_{1,2}$ depend on the angle of the leptons w.r.t to the decay axis in the q -RF,

$$\begin{aligned} \ell_1^{(2)} &= (\gamma(E_{\ell_1}^{(3)} + \beta \cos \theta_\ell |\vec{\ell}_1^{(3)}|), \gamma(\beta E_{\ell_1}^{(3)} + \cos \theta_\ell |\vec{\ell}_1^{(3)}|), -|\vec{\ell}_1^{(3)}| \sin \theta_\ell, 0), \\ \ell_2^{(2)} &= (\gamma(E_{\ell_2}^{(3)} - \beta \cos \theta_\ell |\vec{\ell}_1^{(3)}|), \gamma(\beta E_{\ell_2}^{(3)} - \cos \theta_\ell |\vec{\ell}_1^{(3)}|), +|\vec{\ell}_1^{(3)}| \sin \theta_\ell, 0), \end{aligned} \quad (\text{A.4})$$

where $E_{\ell_{1,2}}^{(3)}$ and $|\vec{\ell}_1^{(3)}|$ are quantities defined in the q -RF:

$$E_{\ell_{1,2}}^{(3)} = \sqrt{|\vec{\ell}_1^{(3)}|^2 + m_{\ell_{1,2}}^2} = \frac{1}{2q} (q^2 + m_{\ell_{1,2}}^2 - m_{\ell_{2,1}}^2), \quad |\vec{\ell}_1^{(3)}| = \frac{\lambda^{1/2}(q^2, m_{\ell_1}^2, m_{\ell_2}^2)}{2q}. \quad (\text{A.5})$$

The boost velocity β and γ -factor are given by

$$\beta = \frac{|\vec{p}_K^{(2)}|}{E_q^{(2)}}, \quad \gamma = \frac{1}{\sqrt{1 - \beta^2}} = \frac{E_q^{(2)}}{q}. \quad (\text{A.6})$$

B. More Detail on the Charm Parameterisation

Here we give some more detail on the charm parameterisation (4.5) used in this paper. The perturbative evaluation of $\Delta C_9(q^2)$ reads

$$\Delta C_9(q^2) = (C_2 + 3C_1)h_c(q^2) - \frac{\alpha_s}{4\pi} \sum_{i=1,2} C_i F_i^{(9)}(q^2) + \mathcal{O}(\alpha_s^2, C_{3,6}), \quad (\text{B.1})$$

where h_c is vacuum polarisation ($\text{Im}[h_c(s)] = \frac{\pi}{3}R(s)$ with $R(s) \equiv \frac{\sigma(e^+e^- \rightarrow \text{hadrons})}{\sigma(e^+e^- \rightarrow \mu^+\mu^-)}$ an experimentally well-studied ratio of cross sections [26]), reproduced in [27] for example, and the second term includes b s c c -vertex corrections not captured by the first term. For the latter, we have adapted the notation and results from the inclusive mode $b \rightarrow s \ell \ell$ [23]. This treatment falls short of effects specific to the structure of the \bar{B} - and \bar{K} -mesons. The Wilson coefficients $C_{3,6}$ correspond to the penguin induced four quark operators and can be neglected for our purposes. The $C_2 \approx 1$ Wilson coefficient arises at tree level and $C_1 \approx -0.15$ is generated by renormalisation group running (specifically we employ $(C_1, C_2, C_9)(m_b) = (-0.15, 1, 4.035)$ as reference values). The combination $C_2 + 3C_1 \approx 0.6$ is referred to as the colour suppressed contribution whereas the radiative corrections are colour enhanced and reduce the LO corrections considerably. In our numerical analysis we use single subtracted points at $\Delta C_9(0 \text{ GeV}^2) \approx 0.27 + 0.073i$ and $\Delta C_9(1 \text{ GeV}^2) \approx 0.24 + 0.031i$.

We turn to the input into the dispersion integral which is the discontinuity. Let us clarify the approximations used. In the case of infinitely narrow resonances and further assuming naïve factorisation (NF) one has, $(2\pi i)^{-1} \text{disc}[\Delta C_9]_{\text{NF}}(s) = \frac{3\pi}{\alpha^2}(C_2 + 3C_1)m_\Psi \Gamma_{\Psi \rightarrow \ell^+\ell^-} \delta(s - m_\Psi^2)$. In this limit, one can correct for NF by multiplying the amplitude by a complex number $\rho_\Psi e^{i\delta_\Psi}$ ($\rho_\Psi \geq 0$),

$$\frac{1}{2\pi i} \text{disc}[\Delta C_9](s) \Big|_{\frac{\Gamma_\Psi}{m_\Psi} \rightarrow 0} = \frac{3\pi}{\alpha^2}(C_2 + 3C_1) \rho_\Psi e^{i\delta_\Psi} m_\Psi \Gamma_{\Psi \rightarrow \ell^+\ell^-} \delta(s - m_\Psi^2) + \dots, \quad (\text{B.2})$$

which parameterises its deviation. Turning to the more realistic case of finite widths, the dispersion integral in (4.4) assumes the form

$$\begin{aligned} \frac{(q^2 - s_0)^n}{2\pi i} \int_{\text{cut}}^{\infty} \frac{ds}{(s - s_0)^n} \frac{\text{disc}[\Delta C_9](s)}{s - q^2 - i0} = \\ - \frac{3\pi}{\alpha^2}(C_2 + 3C_1) \sum_{r \in \Psi} \left(\frac{q^2 - s_0}{m_r^2 - s_0} \right)^n \frac{\rho_r e^{i\delta_r} m_r \Gamma_{r \rightarrow \ell^+\ell^-}}{q^2 - m_r^2 + i m_r \Gamma_r} + \dots \end{aligned} \quad (\text{B.3})$$

As previously mentioned the dots stand for neglected multi-hadron contributions which start at $q^2 = 4m_D^2$. At last, let us comment on the status of the resonance data, the significance of writing the dispersion relation in ΔC_9 rather than the amplitude and parameterising without reference to the SM.

- From the branching fractions, it has been known for a long time that $\rho_{J/\Psi} \approx 1.38$ and $\rho_{\Psi(2S)} \approx 1.56$ and that there are sizeable corrections to NF. By fitting the interference of the (broad) charm resonances with the short distance contributions, the corresponding correction factors were found to be even larger and come with opposite phase $\delta_\Psi \approx \pi$ as compared to NF [27] (cf. plots and tables therein). Later, the LHCb collaboration [29] fitted the phases of the J/Ψ - and $\Psi(2S)$ -resonances which are more challenging as they are narrow. Qualitatively, a four fold degeneracy $(\delta_{J/\Psi}, \delta_{\Psi(2S)}) \approx (\pm \frac{\pi}{2}, \pm \frac{\pi}{2})$ (cf. Tab. 3 in [29]) emerges which indicates a rather small interference effect since the short distance contribution is real.

- In principle, one could have directly written a dispersion relation for the full amplitude. However, the amplitude and ΔC_9 essentially differ by the form factor $f_+(q^2)$ which is an analytic function with a pole and branch points above the physical region. They are thus both legitimate functions for a dispersion relation. Differences comes into play when approximations are made. In our case, they differ on how we extend from the narrow resonance limit, which is not-known from first principles, and thus, a priori, any of the two seems as good as the other. Perhaps, the one for ΔC_9 is preferable as we know that the extension is at least correct in the case of NF, which might be seen as a reasonable qualitative starting point.
- One may parameterise without reference to NF (cf. Eq. (3) in [29])

$$\frac{1}{2\pi i} \text{disc}[\Delta C_9](s) = \eta_r e^{i\delta_r} m_r \Gamma_r \delta(s - m_r^2), \quad (\text{B.4})$$

thereby avoiding reference to the SM. Comparison with (B.2) reveals the relation between the parameters

$$\eta_r \Gamma_r = \rho_r \frac{3\pi}{Q^2} (C_2 + 3C_1) \Gamma_{r \rightarrow \ell^+ \ell^-}. \quad (\text{B.5})$$

C. Supplementary plots

In this appendix, we provide a few supplementary plots which might be of interest to certain readers of the paper. This includes the MC-plots in Figs. 7 about angular distributions. The fact that QED gives rise to qualitatively different angular distribution (or higher moments) was pointed out in [32] (cf. Sec. 5) and advertised as a way to measure pure QED effects. Auxiliary plots for the semi-analytic approach are shown in Figs. 8 and 9 which can help to better understand the normalised figures since the normalisation depends on the charm input.

D. Values of f^{th} used in the Monte Carlo Simulations

Tab. 3 gives the values of $\frac{\Gamma_3}{\Gamma_{\text{tree}}}$ for various cases, which are used to calculate f^{th} , needed for the normalisation of the Monte Carlo.

When the resonance is “off”, only the contribution from the rare mode is considered, and the integration for the total rates is performed over the full range of q_0^2 . In this case, we consider two possible frames (\bar{p}_B and q_0) for imposing the spurious cut on the photon energy $E_\gamma^{(i)}$ in order to separate 3- and 4-body events. We note that the coefficient of the soft log ($\ln E_\gamma^{(i)}$) is the same for each case, as expected. The results are given for 3 different leptons (μ , $10e$ and e) for each photon energy cut. The shorthand $10e$ denotes an “intermediate” lepton which has a mass of $m_{10e} = 10 m_e$, which is roughly in between the muon and electron mass.

When the resonance is “on”, the contribution from the interference of the rare mode with the Breit-Wigner term of the J/ψ is included, but not the square of the Breit-Wigner term itself. In this case, we consider two possible values for the phase of the J/ψ : $\delta_{J/\psi} = 0$

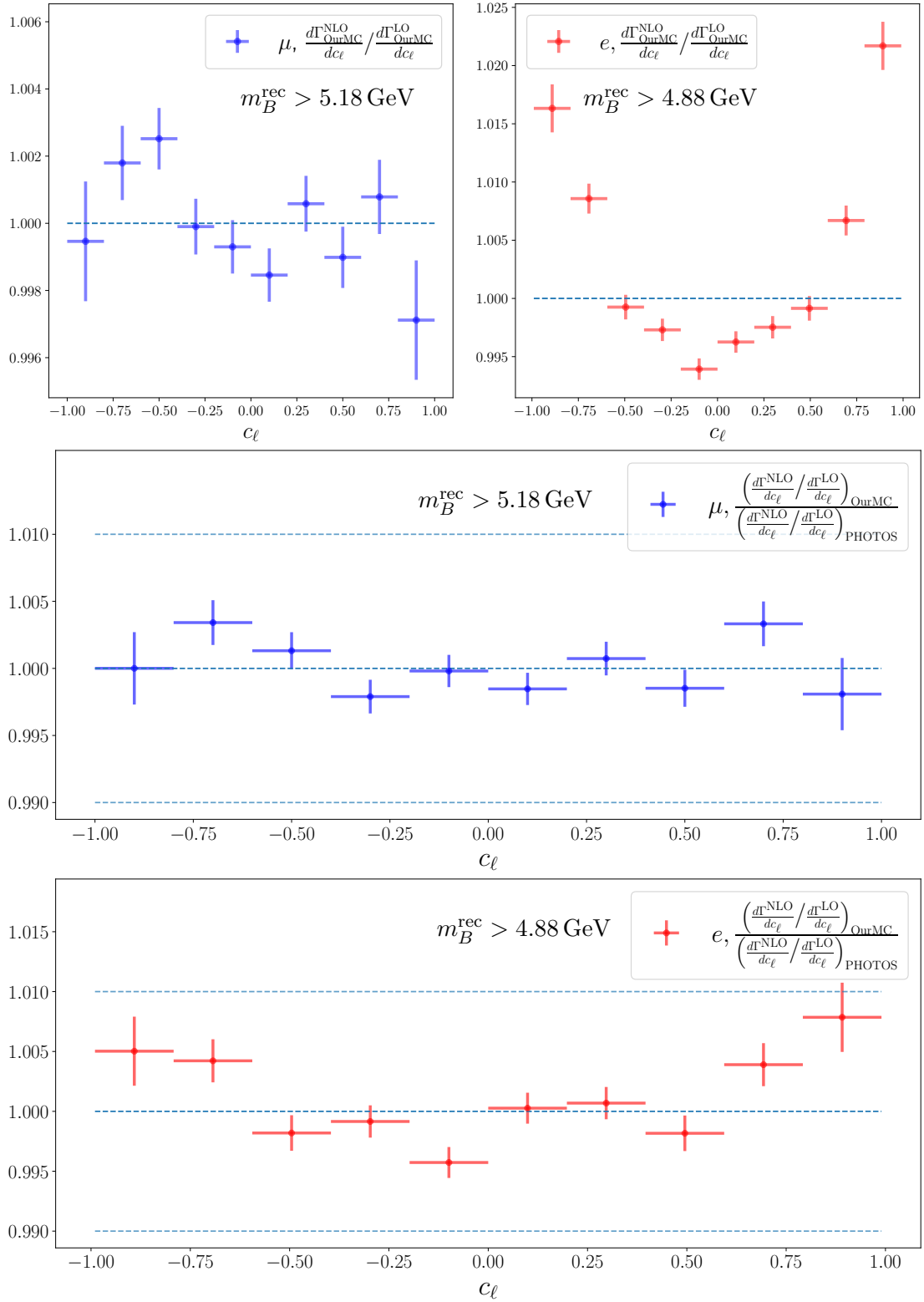


Figure 7. Short distance (form factor) plots, in the c_ℓ -variable, NLO over LO for muons in blue (top left) and for electrons in red (top right) in our MC, with appropriate cuts as in Tab. 1. The normalisation of these plots is not meaningful (cf. main text). However, double ratios, shown in the middle and bottom, of our Monte Carlo versus the PHOTOS framework are free of ambiguities.

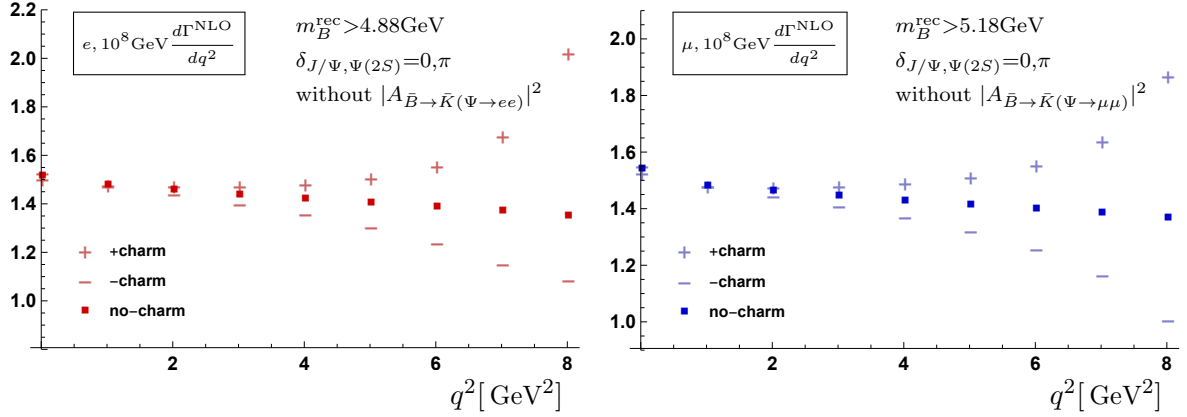


Figure 8. Same plots as in Fig. 5 without LO-normalisation.

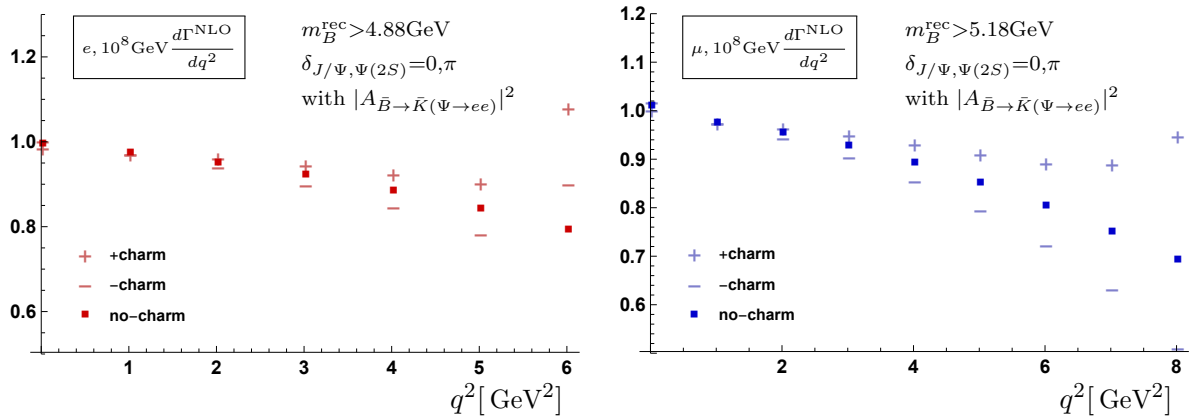


Figure 9. Same plots as in Fig. 6 without LO-normalisation.

(maximum interference) and $\delta_{J/\psi} = 1.47$ (LHCb value from [29]). The corresponding restrictions on the range of the q_0^2 integration are $q_0^2 \leq 9.5905 \text{ GeV}^2$ and $q_0^2 \leq 9.585 \text{ GeV}^2$ respectively. This is done in order to capture the maximum effect from the interference term in each case. Only results for photon energy cuts in the q_0 -RF are given, since in the \bar{p}_B -RF, the MC has extremely low efficiency. This is because for a photon energy cut-off in the \bar{p}_B -RF, the sampling for the MC also has to be performed in \bar{p}_B . Then, applying a cut in q_0^2 (which is now a function of several sampling variables) becomes problematic, and significantly decreases the sampling efficiency. Furthermore, having an electron mass also significantly decreases the efficiency of the Monte Carlo, so we restrict ourselves to a muon mass m_μ and an “intermediate” mass $m_{10e}(= 10m_e)$ when interference effects are considered.

References

- [1] M. Artuso, G. Isidori, and S. Stone, *Searching for New Physics in b decays*. World Scientific, 2022.
- [2] S. Bifani, S. Descotes-Genon, A. Romero Vidal, and M.-H. Schune, “Review of Lepton

Resonance	Frame for $E_{\gamma,\text{cut}}^{(i)}$	Lepton	$\frac{\Gamma_3}{\Gamma_{\text{tree}}}$
Off	$\bar{p}B$	μ	$1 + \frac{\alpha}{\pi} \left(5.1479 + 10.924 \ln E_{\gamma,\text{cut}}^{(\bar{p}B)} \right)$
		$10e$	$1 + \frac{\alpha}{\pi} \left(7.8551 + 23.012 \ln E_{\gamma,\text{cut}}^{(\bar{p}B)} \right)$
		e	$1 + \frac{\alpha}{\pi} \left(9.9605 + 32.222 \ln E_{\gamma,\text{cut}}^{(\bar{p}B)} \right)$
	q_0	μ	$1 + \frac{\alpha}{\pi} \left(6.8903 + 10.924 \ln E_{\gamma,\text{cut}}^{(q_0)} \right)$
		$10e$	$1 + \frac{\alpha}{\pi} \left(12.473 + 23.012 \ln E_{\gamma,\text{cut}}^{(q_0)} \right)$
		e	$1 + \frac{\alpha}{\pi} \left(16.772 + 32.222 \ln E_{\gamma,\text{cut}}^{(q_0)} \right)$
On, $\delta_{J/\psi} = 0$	q_0	μ	$1 + \frac{\alpha}{\pi} \left(8.7111 + 10.140 \ln E_{\gamma,\text{cut}}^{(q_0)} \right)$
		$10e$	$1 + \frac{\alpha}{\pi} \left(16.658 + 22.223 \ln E_{\gamma,\text{cut}}^{(q_0)} \right)$
On, $\delta_{J/\psi} = 1.47$	q_0	μ	$1 + \frac{\alpha}{\pi} \left(9.6159 + 9.5767 \ln E_{\gamma,\text{cut}}^{(q_0)} \right)$
		$10e$	$1 + \frac{\alpha}{\pi} \left(19.271 + 21.647 \ln E_{\gamma,\text{cut}}^{(q_0)} \right)$

Table 3. f^{th} for different cases. When the resonance is “on”, the interference of the Breit-Wigner term of the J/ψ and the rare mode is included (but not the square of the Breit-Wigner term). $10e$ is a ‘fake’ lepton that has an ‘intermediate’ mass (between the muon and the electron), and we take $m_{10e} = 10 m_e$. When the resonance is “off” (ie. only rare mode), the full range of q_0^2 is integrated over. When $\delta_{J/\psi} = 0$, the q_0^2 integration is restricted in the region $q_0^2 \leq 9.5905 \text{ GeV}^2$, whereas when $\delta_{J/\psi} = 1.47$, the q_0^2 integration is restricted in the region $q_0^2 \leq 9.585 \text{ GeV}^2$. $E_{\gamma,\text{cut}}^{(i)}$ is given in GeV units.

Universality tests in B decays,” *J. Phys. G* **46** no. 2, (2019) 023001, [arXiv:1809.06229 \[hep-ex\]](#).

- [3] G. Hiller and F. Kruger, “More model-independent analysis of $b \rightarrow s$ processes,” *Phys. Rev. D* **69** (2004) 074020, [arXiv:hep-ph/0310219](#).
- [4] M. Bordone, G. Isidori, and A. Pattori, “On the Standard Model predictions for R_K and R_{K^*} ,” *Eur. Phys. J. C* **76** no. 8, (2016) 440, [arXiv:1605.07633 \[hep-ph\]](#).
- [5] G. Isidori, S. Nabeebaccus, and R. Zwicky, “QED corrections in $\bar{B} \rightarrow \bar{K} \ell^+ \ell^-$ at the double-differential level,” *JHEP* **12** (2020) 104, [arXiv:2009.00929 \[hep-ph\]](#).
- [6] **LHCb** Collaboration, R. Aaij *et al.*, “Test of lepton universality using $B^+ \rightarrow K^+ \ell^+ \ell^-$ decays,” *Phys. Rev. Lett.* **113** (2014) 151601, [arXiv:1406.6482 \[hep-ex\]](#).
- [7] **LHCb** Collaboration, R. Aaij *et al.*, “Search for lepton-universality violation in $B^+ \rightarrow K^+ \ell^+ \ell^-$ decays,” *Phys. Rev. Lett.* **122** no. 19, (2019) 191801, [arXiv:1903.09252](#)

- [hep-ex].
- [8] **LHCb** Collaboration, R. Aaij *et al.*, “Test of lepton universality in beauty-quark decays,” [arXiv:2103.11769](#) [hep-ex].
- [9] **LHCb** Collaboration, R. Aaij *et al.*, “Test of lepton universality with $B^0 \rightarrow K^{*0} \ell^+ \ell^-$ decays,” *JHEP* **08** (2017) 055, [arXiv:1705.05802](#) [hep-ex].
- [10] **LHCb** Collaboration, R. Aaij *et al.*, “Tests of lepton universality using $B^0 \rightarrow K_S^0 \ell^+ \ell^-$ and $B^+ \rightarrow K^{*+} \ell^+ \ell^-$ decays,” [arXiv:2110.09501](#) [hep-ex].
- [11] E. Barberio, B. van Eijk, and Z. Was, “PHOTOS: A Universal Monte Carlo for QED radiative corrections in decays,” *Comput. Phys. Commun.* **66** (1991) 115–128.
- [12] E. Barberio and Z. Was, “PHOTOS: A Universal Monte Carlo for QED radiative corrections. Version 2.0,” *Comput. Phys. Commun.* **79** (1994) 291–308.
- [13] P. Golonka and Z. Was, “PHOTOS Monte Carlo: A Precision tool for QED corrections in Z and W decays,” *Eur. Phys. J. C* **45** (2006) 97–107, [arXiv:hep-ph/0506026](#).
- [14] N. Davidson, T. Przedzinski, and Z. Was, “PHOTOS interface in C++: Technical and Physics Documentation,” *Comput. Phys. Commun.* **199** (2016) 86–101, [arXiv:1011.0937](#) [hep-ph].
- [15] M. Schonherr and F. Krauss, “Soft Photon Radiation in Particle Decays in SHERPA,” *JHEP* **12** (2008) 018, [arXiv:0810.5071](#) [hep-ph].
- [16] **Sherpa** Collaboration, E. Bothmann *et al.*, “Event Generation with Sherpa 2.2,” *SciPost Phys.* **7** no. 3, (2019) 034, [arXiv:1905.09127](#) [hep-ph].
- [17] F. U. Bernlochner and M. Schonherr, “Comparing different ansatzes to describe electroweak radiative corrections to exclusive semileptonic B meson decays into (pseudo)scalar final state mesons using Monte-Carlo techniques,” [arXiv:1010.5997](#) [hep-ph].
- [18] S. Calí, S. Klaver, M. Rotondo, and B. Sciascia, “Impacts of radiative corrections on measurements of lepton flavour universality in $B \rightarrow D \ell \nu_\ell$ decays,” *Eur. Phys. J. C* **79** no. 9, (2019) 744, [arXiv:1905.02702](#) [hep-ph].
- [19] S. Weinberg, “Infrared photons and gravitons,” *Phys. Rev.* **140** (1965) B516–B524.
- [20] J. Eschle, A. Puig Navarro, R. Silva Coutinho, and N. Serra, “zfit: scalable pythonic fitting,” [arXiv:1910.13429](#) [physics.data-an].
- [21] A. Ryd, D. Lange, N. Kuznetsova, S. Versille, M. Rotondo, D. P. Kirkby, F. K. Wuerthwein, and A. Ishikawa, “EvtGen: A Monte Carlo Generator for B-Physics,”.
- [22] M. Dobbs and J. B. Hansen, “The HepMC C++ Monte Carlo event record for High Energy Physics,” *Comput. Phys. Commun.* **134** (2001) 41–46.
- [23] H. H. Asatrian, H. M. Asatrian, C. Greub, and M. Walker, “Two loop virtual corrections to $B \rightarrow X_s \ell^+ \ell^-$ in the standard model,” *Phys. Lett. B* **507** (2001) 162–172, [arXiv:hep-ph/0103087](#).
- [24] P. Ball and R. Zwicky, “New results on $B \rightarrow \pi, K, \eta$ decay formfactors from light-cone sum rules,” *Phys. Rev. D* **71** (2005) 014015, [arXiv:hep-ph/0406232](#).
- [25] **LHCb** Collaboration, R. Aaij *et al.*, “Test of lepton universality using $B^+ \rightarrow K^+ \ell^+ \ell^-$ decays,” *Phys. Rev. Lett.* **113** (2014) 151601, [arXiv:1406.6482](#) [hep-ex].

- [26] **Particle Data Group** Collaboration, M. Tanabashi *et al.*, “Review of Particle Physics,” *Phys. Rev.* **D98** no. 3, (2018) 030001.
- [27] J. Lyon and R. Zwicky, “Resonances gone topsy turvy - the charm of QCD or new physics in $b \rightarrow s\ell^+\ell^-?$,” [arXiv:1406.0566 \[hep-ph\]](#).
- [28] C. Cornella, G. Isidori, M. König, S. Liechi, P. Owen, and N. Serra, “Hunting for $B^+ \rightarrow K^+\tau^+\tau^-$ imprints on the $B^+ \rightarrow K^+\mu^+\mu^-$ dimuon spectrum,” *Eur. Phys. J. C* **80** no. 12, (2020) 1095, [arXiv:2001.04470 \[hep-ph\]](#).
- [29] **LHCb** Collaboration, R. Aaij *et al.*, “Measurement of the phase difference between short- and long-distance amplitudes in the $B^+ \rightarrow K^+\mu^+\mu^-$ decay,” *Eur. Phys. J. C* **77** no. 3, (2017) 161, [arXiv:1612.06764 \[hep-ex\]](#).
- [30] S. Nabeebaccus and R. Zwicky, *to appear*.
- [31] R. Zwicky, “QED-Corrections to Weak Decays,” *Symmetry* **13** no. 11, (2021) 2036, [arXiv:2205.06194 \[hep-ph\]](#).
- [32] J. Gratrex, M. Hopfer, and R. Zwicky, “Generalised helicity formalism, higher moments and the $B \rightarrow K_{J_K}(\rightarrow K\pi)\bar{\ell}_1\ell_2$ angular distributions,” *Phys. Rev.* **D93** no. 5, (2016) 054008, [arXiv:1506.03970 \[hep-ph\]](#).